Guide to Ground Penetrating Radar Survey for Detection of Underground Utilities

Acknowledgements

FOREWORD

After the disastrous landslip of 1994 occurred in Kwun Lung Lau on Hong Kong Island, the Government has paid more attention on utility maintenance with particular emphasis on leakage detection of buried water carrying services on both slopes and roads. The Government has increased resources and imposed additional legislation on the detection of underground utilities. As a direct result, the utility profession has been developing rapidly, and over the last decade, the number of "Utility Specialists" (管綫專業監理師) has grown as the Government's requirements for Competent Persons to carry out the investigations has been implemented, in addition, Recognized Professional Utility Specialist (RPUS) (管綫專業監察師) has been recognized in recent years. However, lack of standard surveying methods, centralized monitoring systems and organized management, have lead to unsatisfactory investigation results.

In order to address these issues, Hong Kong Institute of Utility Specialists (HKIUS) (香港管綫專業學會), targeting the promotion of knowledge and good practice in the utility profession, collaborated with Hong Kong Utility Research Centre (HKURC) and supported by the funding from the Professional Services Development Assistance Scheme (PSDAS) of HKSAR, published a series of guide books and pamphlets in 12 disciplines of the utility profession in order to set standards for the practitioners to follow. As part of HKIUS continual effort to enhance the professionalism of the utility profession, it is the intention of the series that the quality of the survey can be raised and that utility related incidents can be avoided by performing high quality utility practices. Hopefully, the resulting benefits can extend to the general public.

This issue provides good practice of using Ground Penetrating Rader (GPR)(管綫雷達探測) in Utility Survey. It states the whole process and specification of conducting GPR from planning to finishing stages and intended to be used by all personnel involved in the works.

_____

Mr, Zico Kai Yip KWOK
(郭啟業先生)
President, HKIUS (2010-11)
April, 2011

Table of Content

1. INTRODUCTION

The first application of ground penetrating radar (GPR) survey was to determine the depth of a glacier, reported in 1929 (Stern, 1929, 1930). Then the technology was lost until the late 1950's when planes crashing into the Greenland ice cap reawakened the interest in the subject (see further history in Clarke, 1987; Young, 1996). Since the mid-1980's, ground penetrating radar has become very popular, particularly for engineering, environmental and archaeological application (Albert and etc, 2000).

The 1929 method of radiointerferometry was independently rediscovered for the 1972 Apollo 17 mission to the moon (Simmons et al., 1972). Most ground penetrating radar systems today are short impulse time domain systems similar to Barringer (1965) or Caldecott (1967) and used in simple imaging mode to map subsurface events, such as the occurrence of the water table (Barringer, 1966; Caldecott et al., 1972; Morey, 1974; Beres and Hasni, 1991), hazardous waste investigations (Brewster and Annan, 1994), mapping sediment sequences (Smith and Hol, 1997), detection of buried objects in conjunction with other methods (Annan et al., 1990; Stockbauer and Kalinec, 1995; Czarnowski et al., 1994; Graf, 1989; Tong, 1993; Powers and Olhoeft, 1996), road pavement evaluation, void detection, behind tunnel linings (Albert and etc, 2000) and detection of fractures in limestone (M. Grasmueck et al., 2005), stratigraphy in beach sand (M. Grasmueck et al., 2006), tree roots and building foundations (M. Grasmueck et al., 2006; A. Novo et al., 2008).

However, large scale investigations in Hong Kong have focused on properties of concrete (W.L. Lai et al., 2009) which is applied on large aboveground infrastructure like bridge, dam and so on. This guideline is trying to summarize the oversea nature experience and theory for reference to the interested person in utility industry.

2. PRINCIPLE OF OPERATION

This chapter is designed as a basic introduction to some of the key concepts in the basic theory of operation of ground-penetrating radar (GPR) and GSSI SIR System will be taken for explanation. An understanding of the concepts discussed here will help make your understanding much more worthwhile and enable you to save more time.

2.1 Equipment

A GPR system is made up of three main components: the control unit, antenna, and power supply which are shown in Figure 2.1.
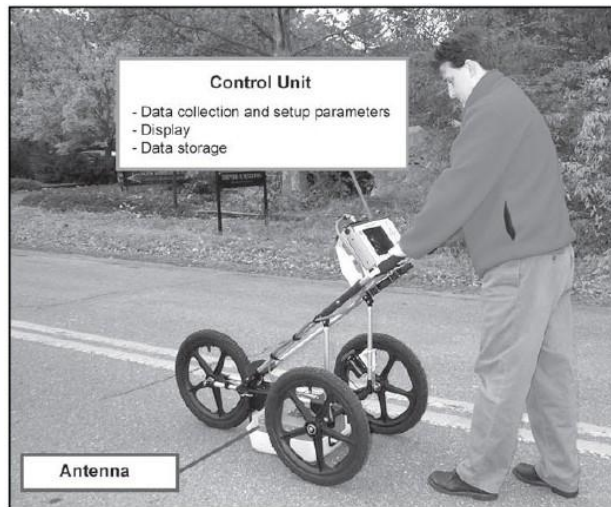
Figure 2.1: Complete GPR system produced by Geophysical Survey Systems, Inc. (USA)

Geophysical Survey Systems GPR equipment can be run with a variety of power supplies ranging from small rechargeable battery packs, to vehicle batteries, and normal 110-volt current. Connectors and adapters are available for each power source type. The unit in the photo above can run from a small internal rechargeable battery or external power. The control unit contains electronics that produce and regulate the pulse of radar energy that the antenna sends into the ground. It also has a built-in computer and hard disk to record and store data for examination after fieldwork. Some systems, such as the GSSI SIR-20, are controlled by an attached Windows laptop computer with pre-loaded control software. This system allows data processing and interpretation without having to download radar files to another computer.

The antenna receives the electrical pulse produced by the control unit, amplifies it, and transmits it into the ground or other medium at a particular frequency. Antenna frequency is a major factor in depth penetration. The higher the frequency of the antenna, the shallower into the ground it will penetrate. A higher frequency antenna will also 'see' smaller targets. Antenna choice is one of the most important factors in survey design. Table 2.1 shows antenna frequency, approximate depth penetration, and appropriate application.

Depth Range (Approximate)	Primary Antenna Choice	Secondary Antenna Choice	Appropriate Application
0-0.5 m	1500 MHz	900 MHz	Structural Concrete, Roadways, Bridgedecks
0-1 m	900 MHz	400 MHz	Concrete, Shallow soils, Archaeology
0-3 m	400 MHz	200 MHz	Shallow Geology, Utilities, UST's, Archaeology
0-9 m	200 MHz	100 MHz	Geology, Environmental, Utility, Archaeology
0-30 m	100 MHz	Sub-Echo 40	Geologic Profiling
Greater than 30 m	MLF (80, 40, 32, 20, 16 MHz)	-	Geologic Profiling

Table 2.1: Choosing the Proper Antenna

2.2 The GPR Method: Theory of Operation

GPR works by sending a pulse of energy into a material and recording the strength and the time required for the return of any reflected signal. A series of pulses over a single area make up what is called a scan, or sometimes a trace. Reflections are produced whenever the energy pulse enters into a material with different electrical conduction properties (dielectric permittivity) from the material it left. The strength or amplitude of the reflection is determined by the contrast in the dielectric constants of the two materials. This means that a pulse which moves from dry sand (diel of 5) to wet sand (diel of 30) will produce a very strong, brilliantly visible reflection, while one moving from dry sand (5) to limestone (7) will produce a very weak reflections.

While some of the energy is reflected back to the antenna, energy also keeps traveling through the material until it either dissipates (attenuates) or the GPR control unit has closed its time window (Figure 2.2). The rate of signal attenuation varies widely and is dependant on the dielectric properties of the material through which the pulse is passing. Another concern is conductivity. Materials which are highly conductive and thus attenuate (absorb) the signal rapidly. If the signal is absorbed, then it is not allowed to penetrate deeper into a material. Water saturation dramatically raises the dielectric (and sometimes the conductivity) of a material, so a survey area should be carefully inspected for signs of water penetration. Radar surveys should never be conducted through standing water, no matter how shallow. Depth penetration through a material with a high dielectric will not be very good. Metals are considered to be a complete reflector, and do not allow any amount of signal to pass through. Materials beneath a metal sheet, fine metal mesh, or pan decking will not be visible. It is essential to correctly estimate the dielectric constant of a material in order to get accurate depth calculations to features. In utility and concrete inspection work, this is commonly done by drilling or chipping to a known object such as a piece of rebar, measuring the depth, and calibrating that depth to the radar record. The depth accuracy of radar is extremely good if this calibration is performed. If there is a suspicion of changing conditions in the subsurface (different material, water infiltration), another depth calibration for that area should be done. Generally speaking, the more depth calibrations are performed, the more accurate the depth is estimated. If chipping or drilling is not possible, or if the survey takes place out of doors on a natural ground surface, the dielectric must be estimated. A chart of the dielectric constants of some common materials is included at the back of this booklet for reference.
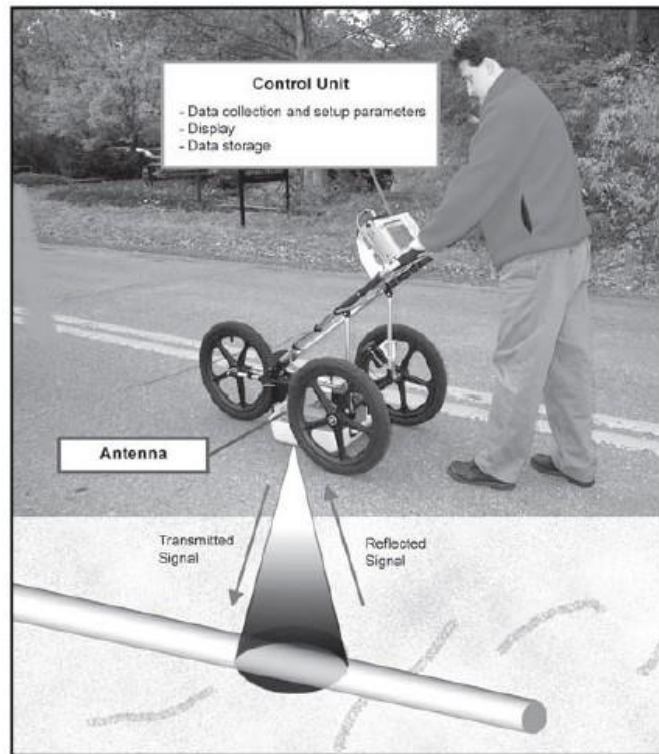
Figure 2.2 Signal path of antenna.

Radar energy is emitted from the antenna not in a straight line, but a cone (Figure 2.3). The two-way travel time for energy at the leading edge of the cone is longer than for energy directly beneath the antenna. This is because that leading edge of the cone represents the hypotenuse of a right triangle. It is a longer distance than when the antenna is directly over the target. Because it takes longer for that energy to be received, it is recorded farther down in the profile. As the antenna is moved over a target, the distance between them decreases until the antenna is over the target, and increases as the antenna is moved away. It is for this reason that a single target will appear in a data as a hyperbola, or inverted "U." The target is actually at the peak amplitude of the positive wavelet. A mathematical function called migration may be performed during the data processing stage to remove the tails of the hyperbola and produce a more accurate assessment of the target location.
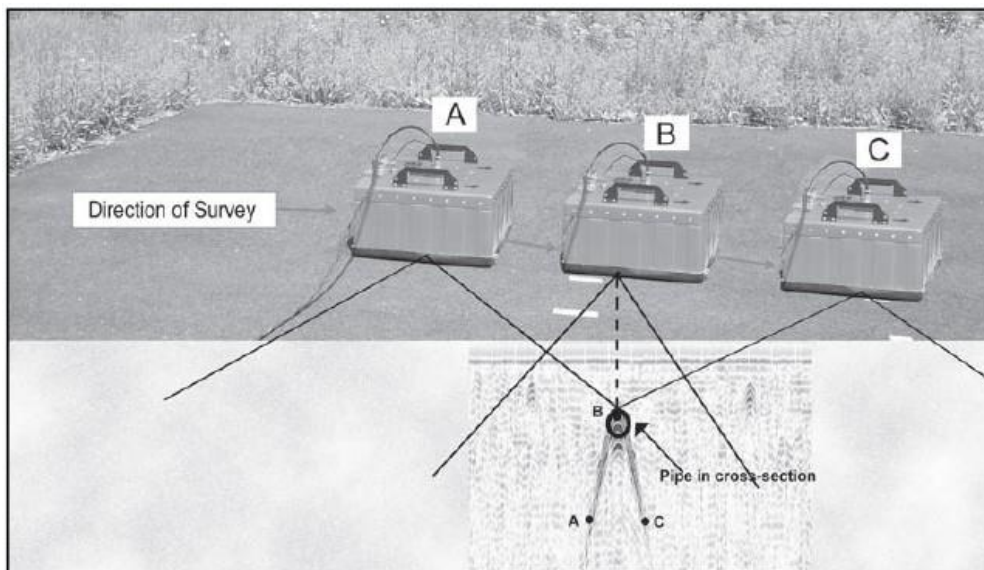
Figure 2.3 Hyperbola creation.

A reflection wave commonly has a positive and a negative wavelet. This is why hyperbolas look striped. If radar energy moves into air (dielectric of 1) from a higher dielectric medium like concrete, the signal will undergo what is called a phase reversal. A normal reflection will exhibit first a positive peak (white band) and then a negative peak (black band), while a phase-shifted signal will show a negative (black) than positive (white) peak. If energy penetrates a thin slab and continues into the air behind it, then a phase shift may indicate the back of the slab. Additionally, voids and air-filled PVC, if they are large enough, may show up as phase-shifted reflections. In some cases however, a phase shift may be falsely produced by background noise or the system's internal filters. It is therefore inadvisable to consider a phase shift alone to be indicative of a void or PVC piping.

2.3 Survey Considerations

Ground-penetrating radar, like all geophysical techniques, is the most effective when as large an area as possible is surveyed. The reason for this is that effective interpretation depends on seeing contrasts within the data. Furthermore, features at the edge of the survey area may not be seen as clearly, and it is preferable to take a slightly longer time to complete the survey, then to make a costly, potentially dangerous mistake because of an inadequate survey area. If there is to be a delay between survey and any drilling or cutting, then some methods of relocating the survey area and mapped features must be devised. Survey areas can be marked on the floor in permanent marker, or the survey area's location in reference to some immobile object such as drill hole or a column should be mapped.

Example:
A fiber optic cable is to be laid into a warehouse floor. The slab contains 8-inch on center rebar mesh and live power conduits in PVC laid on top of the mesh. The trench is to be 8 inches wide and dug to the top of the mesh. The client wants the conduit laid on top of the mesh, so accurate depth calculation to top of mesh is essential. Multiple drill cores to mesh are permitted for depth calibration. While it is possible to survey only the area that will be directly impacted, a much more effective technique would be to survey an additional 12 inches to the sides of the trench. This will help in the identification of targets at the edge of the trench. Cores should be taken down to the mesh all along the impact area.

GPR functions by transmitting and receiving electromagnetic energy at a particular frequency. Cellular phones, two-way radios, and pagers also transmit EM energy and will interfere with a GPR survey. If you must have them on, it is absolutely essential to keep these devices at least 25- 30 feet away from the antenna.

2.4 Data Processing

Many situations will require the operator only to note the location of a target so that it can be avoided. For these clients, it may only be necessary to use a simple linescan format and mark the approximate area on the survey surface. Other clients may require detailed subsurface maps and depth to features. These situations will require the operator to use GSSI software to apply different mathematical functions to the data to remove background interference, migrate hyperbolas, and calculate accurate depth. With some GSSI systems, such as the StructureScan concrete analysis system, this is automated. Other situations may require a greater understanding of radar processing techniques, and the operator may wish to refer to the coming manual of ground penetrating radar survey for detection of underground utilities.

2.5 Principle of GPR

Any GPR system includes a signal generator, transmitting and receiver antenna, and a control unit having digital recording facilities. The impulse radar transmits electromagnetic pulses of short duration into the ground from the transmitter antenna. Pulses radiated from the antenna are reflected from various interfaces within the subsurface and are picked-up by the receiver antenna. Radar reflections will be returned from any natural or man-made object that has a contrast in its dielectric properties.

$$D = \varepsilon E$$

The dielectric permittivity relates polarization or electric displacement D to the applied field E

Permittivity is often expressed in terms of the permittivity of free space ε_0 in terms of relative

$$\varepsilon_r = \varepsilon/\varepsilon_0$$

dielectric permittivity
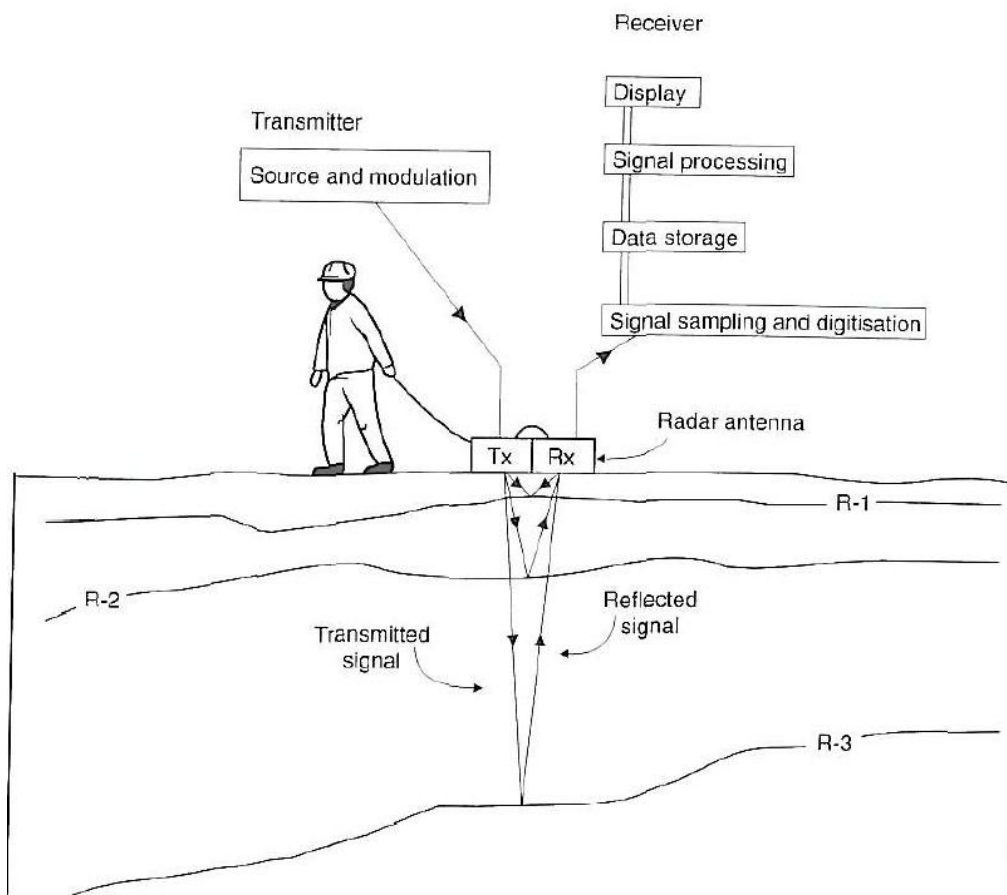
Figure 2.4 Sketch of the basic components of a GPR system and principle of operation.

ε_0 and ε have units of coulombs/volts m or farads/m, whereas ε_r is dimensionless.
ε_r varies from its space value of 1 to a maximum of 80 for water. ε_r is strongly frequency dependent in parts of the electromagnetic spectrum, and should more properly these aspects can be ignored; we will encounter ε_r only at ground penetrating radar frequencies, in range 10 to 1000 MHz.

$$\varepsilon_t = (1 - \phi^3)\varepsilon_s + \phi^3\varepsilon_w$$

With a dielectric permittivity of 80, water dominates the permittivity of rock water mixtures

The speed of radiowaves in any medium is dependent upon the speed of light in free space (c =0.3 m/ns), the relative dielectric constant (εr) and the relative magnetic permeability (μr = 1 for non magnetic materials). The speed of radiowaves in a material (vm) is given by

$$v_m = \frac{c}{\dfrac{\varepsilon_r \mu_r}{2}\left[\sqrt{(1+P^2)}+1\right]}$$

Where:
c   is the speed of light in free space;
εr   is the relative dielectric permittivity;
μr   is the relative magnetic permittivity;
P   is the loss factor, such that $P = \sigma/\omega\varepsilon$;
σ   is the conductivity;
$\omega = 2\pi f$, where f is the frequency;
ε   is the permittivity =$\varepsilon_r\varepsilon_0$, and
ε0   is the permittivity of free space (8.852×10^{-12} F/m).

In low-loss materials, $P \approx 0$ the speed of radiowaves

$$v_m = \frac{c}{\sqrt{\varepsilon_r}} = \frac{0.3}{\sqrt{\varepsilon_r}}$$

The success of ground penetrating radar method relies on the variability of the ground to allow the transmission of radiowaves. Depth of penetration is a function of the radar signal attenuation consist of electrical loses, scattering loses and spreading loses. The primarily factors control electrical attenuation of the electrical conductivity of the subsurface and the radar frequency. An increase in either subsurface conductivity or the radar frequency will result in greater attenuation of the radar signal.

Some materials, such as polar ice, are virtually transparent to radiowaves. Other materials, such as water-saturated clay and saltwater, either absorb or reflect the radiowaves to such an extent that they are virtually opaque to radiowaves. It is the contrast in relative dielectric permittivity between adjacent layers that gives rise to reflection of incident electromagnetic radiation. The greater the contrast, the greater the amount of radiowave energy reflected will be. The proportion of energy reflected, given by the reflection coefficient (R), is determined by the contrast in radiowave velocities, and more fundamentally, by the contrast in the relative dielectric permittivity of adjacent media.

The amplitude reflection coefficient is

$$R = \frac{(v_1 - v_2)}{(v_1 + v_2)}$$

Where $v1$ and $v2$ are the radiowave velocities in layers 1 and 2 respectively, and $v1 < v2$.

Also

$$R = \frac{\sqrt{\varepsilon_2} - \sqrt{\varepsilon_1}}{\sqrt{\varepsilon_2} + \sqrt{\varepsilon_1}}$$

Where $\varepsilon1$ and $\varepsilon2$ are the respective relative dielectric permittivities (εr) of the layers 1 and 2, applicable for incidence at right-angles to a plane reflector assuming no other signal loses and refer to the amplitude of a signal. In all cases the magnitude of R lies in the range +/- 1. The proportion of energy transmitted is equal to 1-R.

GPR antennas are often identified by its approximate centre-band frequency (e.g. 50MHz, 200MHz, etc.). In general, a high frequency antenna has a higher resolution and lower depth penetration (higher attenuation) than low frequency antenna. The transmitter and receiver may be separate, or the same antenna may be utilized to transmit and receive the signal. A system with a separate transmitter and receiver is called bistatic, while a system utilizing the same antenna for transmitter and receiver is monostatic system. High frequency antennas are shielded, so that only the down-ward-directed signal is transmitted and received. Low frequency antennas (<200MHz) are rarely shielded, since it is usually very difficult to absorb that wavelength signal.

3. NUMERICAL MODELING

With wide application of ground penetrating radar survey in Hong Kong, the clear interpretation for radargram should be introduced. Under Professional Service Development Assistance Scheme (PSDAS), the project titled as "Professional Guide Notes and Pamphlet for utility professionals in Hong Kong" will established numerical model of hyperbola in radargram with the help of ray-based monostatic and bistatic modeling algorithms (Cai and McMechan, 1995; Zeng et al., 1995). This technique uses ray tracing to determine propagation paths and integration along these paths to determine traveltimes and amplitudes. The synthetic amplitudes include contributions from the source and receiver directivities, in-plane and out-of-plane geometrical spreading, reflection and transmission coefficients, and attenuation. The directivity used for both transmitter and receiver antennas is that of the far-field of a dipole oriented perpendicular to the survey line (Annan et al., 1973; Engheta et al., 1982).The reflection polarity is positive for reflection at a low-to-high velocity contrast. Reflections that pass through a caustic (e.g., from the bottom of a tank) appear with a phase shift of $\pi/2$.

Ray tracing is fast and efficient. The main limitation on the models is that they are 2.5-dimensions, and the tanks and pipes are assumed to be homogeneous and of infinite length perpendicular to the 2- dimensions plane in which they are defined. The main limitations in the responses are that they do not include off-line effects or wave phenomena such as diffractions.

As an example, Figure 3.1 shows the response of a simple tank model. The tank wall (Figure 3.1c) has a thickness of 5 cm and a diameter of 3 m, and it is buried in silty clay soil with its top 1 m below the earth's surface. It is made of PVC plastic and is empty. The dielectric permittivity and attenuation quality factor for each element in this model are listed in Table 3.1. The corresponding zero-offset ray paths (Figure 3.1b) are used to compute the synthetic GPR profile (Figure 3.1a). Times and amplitudes are interpolated linearly between rays to obtain values at any desired recording points (here equally spaced along the profile). Amplitudes are computed for the nominal frequency of the antenna (200 MHz for this particular example); the source bandwidth is equal approximately to the nominal frequency. Reflections from both the top and bottom of the tank are visible. Free-surface and internal multiples are not simulated.

In this chapter, the responses of 16 different model tank configurations are presented. The model numbers (Table 3.1) are also indicated on the corresponding synthetic radargrams in the following figures. Through these examples, the effects on the GPR response of different tank materials will be investigated.

3.1 Effects of tank materials and contents

Figure 3.2 contains ground penetrating radar (GPR) responses for six tanks with different construction materials and contents. The soil is silty clay and the dominant frequency is 200 MHz. Figure 3.2a is the radargram for three empty tanks made of fiberglass (model 1), PVC (model 2), and metal (model 3). Because the thickness of the tank wall is relatively small compared to its diameter, and the differences of Q (Table 3.1) of the tanks in models 1 and 2 are small, there is no visible amplitude difference in the reflections from the two tank bottoms (D and E). The slight difference of the amplitude of the reflection from the tops of tanks (A and B) may be concealed by noise in real data.

The material used most commonly for the construction of tanks is metal (model 3). The reflection from the top of the metal tank (C in Figure 3.2a) is stronger and of opposite polarity to those from

the tops of the fiberglass and PVC tanks. Neither the reflection (F) from the bottom of a metal tank nor its contents are detectable because of the high reflectivity and high attenuation of the metal.

Figure 3.2b contains the radargrams of three tanks, all made of fiberglass, filled with either the LNAPL benzene (model 4), the DNAPL perchloroethylene (C2Cl4) (model 5), or methanol (model 6). If the tank shape is known, it is possible to differentiate an empty fiberglass tank (model 1) from one that is full of benzene (model 4), or one that is full of C2Cl4 (model 5), from the reflection time differences between the top and the bottom of the tank. The relative reflection times from the bottom of the fluid-filled tanks (G and H) are larger than that for the empty tank (D) because of the different velocities of GPR in the different fluids. Because of the high dielectric constant and low Q (like salt water), a full tank of methanol (model 6) has a totally different response. The polarity of the reflection from the top (I) is reversed, and the reflection from the bottom (J) cannot be seen. This appears very similar to the response of the metal tank, except that the amplitude of the reflection from the top of the tank is smaller (compare with model 3).

3.2 Effects of fluid interfaces within tanks

Figure 3.3 contains the GPR responses of tanks containing two fluids, with the fluid interface in the middle of the tank. The tanks are all made of fiberglass, buried in silty clay, and the radar frequency is 200 MHz. Figure 3.3a shows the response of three tanks with air in the top half, and gasoline (LNAPL), DNAPL, and methanol, respectively, in the bottom half. Although there is about a 20% difference between the dielectric constants of the LNAPL and DNAPL (Table 3.1), the corresponding amplitudes of the reflections (A and B) from the fluid contact within the tanks (models 7 and 8) are visible but not likely to be distinguishable in real data. Although the air/methanol interface (model 9) produces a much larger reflection (C) than either LNAPL or DNAPL does, it is hard to differentiate from salt water (model 12).

Figure 3.3b shows ground penetrating radar (GPR) responses of three tanks with equal amounts of gasoline/water (model 10), air/water (model 11), and air/salt water (model 12). The relative amplitudes and times of the top, fluid interface, and the bottom reflections are sufficiently different for the gasoline/water and air/water configurations that it should be possible to distinguish them. Note particularly, the large reflection times from the tank bottom (F and G for models 10 and 11) when a substantial portion of the tank is filled with water. The existence of a conductive (low Q) fluid (model 12) can be determined easily by the absence of the reflection from the bottom. A quantitative evaluation will be possible if the S/N ratio is sufficiently high.

Figure 3.4 contains the responses of three models (13, 14, and 15 in Table 2.2), at different frequencies, to determine resolution of different fluid levels. The tanks are made of fiberglass and are buried in silty clay. It is not possible to distinguish between the fluid levels greater than 70% (by volume) at 100MHz (Figure 3.4a). However, if the noise is sufficiently low, this frequency can still indicate the existence of air above the fluid by the two high amplitude spots (A) on the reflection from the tank bottom when the fluid level is near 90% (model 15). These spots are the result of focusing produced by differential refraction of rays that intersect the tank wall just above and just below the fluid surface. At 200MHz (Figure 3.4b), the fluid levels up to 80% can be differentiated (compare B and C). At levels higher than this, two high amplitude spots (E) again exist on the reflection from the bottom. At 450 MHz (Figure 3.4c), the reflections from the fluid interfaces (F and G) get closer to the reflection from the top as the fluid level rises, and a distinct reflection (H) is still visible at 95% full. Comparison of the amplitudes in Figures 3.4a, 3.4b, and 3.4c shows that attenuation affects high frequencies more than low; that is, the amplitudes of all reflections become smaller. In Figure 4c, the reflections from the tank bottom are barely visible.

3.3 Effect of tank size

Figure 3.5 shows simulated GPR responses as a function of tank diameter. The three tanks are made of fiberglass, filled with fresh water, and buried in silty clay with their tops at 1.0 m depth (model 16). There are two main diagnostic observations. The first is that the radius of curvature of the reflection from both top and bottom increases as the tank diameter increases. [Migrated images would show the tank radius directly, but are beyond the scope of this chapter]. The second is that the reflections from the top and bottom of the tank become more separated in time as the tank diameter increases. If the tank contents (and hence velocity) are known, the tank size could be calculated from the zero-offset time difference at the apex of the reflections (independent of the material in which the tank is buried).

3.4 Effect of antenna separation

Antenna separation also affects the recorded response in a systematic way. For this example, we consider only the dipole described above. The effect of radiation patterns as a function of offset for other types of antenna (or other dipole orientations) could be similarly simulated. Figure 3.6 shows responses for the 3.0m diameter tank model in Figure 3.5b (model 16), as a function of antenna offset. As offset increases, the traveltimes of both top and bottom reflections increase (because of the increased path length), their separation in time decreases, their radius of curvature increases, and their average amplitude decreases (because of increased geometrical spreading, and attenuation).

More importantly, when the offset is sufficiently wide that the critical refraction angle is exceeded at the free surface, the antenna radiation, and hence the reflections, are of very small amplitude. At 1.0m offset (left side, Figure 3.6), both antennas are in the subcritical regime, and the reflection amplitude is relatively large and a smooth function of position. At 2.0m offset (center, Figure 3.6), rays that are reflected near the top of the tank (see A), are at postcritical angles at both antennas, so the amplitude is small. Rays reflected farther from the top of the tank (at B), are postcritical at only one of the two antennas and therefore give larger amplitudes. At 3.0m offset (right side, Figure 3.6), the incidence angle at the tank top is even wider, and a critical reflection occurs at the soil-to-fiberglass interface and produces both an amplitude increase and a $\pi/2$ phase shift in the reflection (at C). Note also that the relative amplitude of the reflection from the tank bottom increases from 0.0 to 3.0m offset, as it is still in the precritical regime for both antennas. This reflection will undergo the same amplitude changes seen in the reflection from the top (but not the phase shift) at still wider offsets. Reversing the sign of the material property contrast inside and outside the tank would generate the phase shift at the bottom, rather than the top, of the tank. A similar suite of effects occurs for a fixed antenna separation as the depth of target decreases. The radiation pattern is also sensitive to antenna height (Turner, 1994); a raised antenna has a narrower beam width so the amplitude decrease associated with the critical angle occurs at a smaller offset.

3.5 Detection of tank damage

Figure 3.7 shows the effect, on GPR data, of tank damage. As the models are 2.5-dimensions, the damage features are assumed to be of infinite extent perpendicular to the plane of the model cross-sections. Thus "holes" and "dents" are really linear rather than equidimensional. Thus, some of the response characteristics will appear different in real data than in the synthetics. For equidimensional features, the main (in-plane) traveltimes would not change, but the amplitudes and phase would be changed depending on their 3-D shape because of the out-of-plane contributions.

In Figure 3.7, the air-filled tank on the left (model 1) has two "holes" with diameters of 25 cm, one near the top and one near the bottom of the tank. The middle tank is the same as the first, except that it has some gasoline in its bottom below the lower hole (the rest presumably having leaked out). The right tank has two "dents" near its top and bottom. Figure 3.7a shows the synthetic 200 MHz responses to these anomalies. The effect of the hole near the top is hard to see, with the only visible effect a slight shape change (A) of the otherwise perfect hyperbola. The effect of the hole near the bottom (B) is more difficult to see. Both will be concealed by noise in real data. The slight increase in amplitude (C) is caused by the rays reflected from the bottom passing through the upper hole, so the attenuation and transmission loss is less than that of the rays passing through the tank wall.

The small amount of fluid left in the tank is interestingly obvious on the radargram (at D). The effects of dents in the tank (E) are easy to detect with the appropriate frequency. The effect of the lower dent is hard to see, because the energy reflected from the dent is spread instead of being focused. The feature F is caused by rays reflected from the smooth tank bottom that is distorted when passing through the upper dent.

3.6 Effect of noise

Figure 3.8 shows the effect of additive random noise on 200 MHz GPR data. The tank configuration for this example is model 13 (Table 3.2). The lower half of the tank is full of DNAPL; the upper half, air. For comparison, the corresponding noise-free response is shown on the left side of Figure 3.4b. As the signal-to-noise ratio decreases, the ability to detect the reflections (F) from the fluid interface, (B) from the tank bottom, and (T) from the tank top is successively lost.

3.7 Discussion and Conclusions

Ray-based numerical simulations of monostatic and bistatic GPR responses for several tank and pipe configurations reveal the potential for non-invasive diagnostic evaluations. From these preliminary results, it appears that GPR will be useful, not only for tank detection, but also for more detailed in-situ evaluation of their condition and contents.

Simulations are also potentially useful as input to survey design as a guide to choosing an appropriate frequency and antenna separation prior to data acquisition (although it must be remarked that experience has shown that generally some field tests are necessary for optimization at any specific site).

While much can be done with the simplified algorithms used above, they must be considered to be only first-order approximations, especially if details of attenuated and dispersed amplitudes are of interest (Powers and Olhoeft, 1996). Nevertheless, the simulations were able to reproduce the salient features of GPR data recorded over plastic pipes filled with air, fresh water, and salt water, and over a metal pipe as these satisfy the main assumptions in the modeling algorithm.

Of the examples above, those for which the synthetic responses are expected to be least accurate, are those involving tank damage. The reasons are the inability to model truly 3-D features, and because diffractions that would be generated at the corners are not simulated. 3-D modeling is an obvious extension, and is now in development. Diffractions can be simulated by finite-difference solutions (e.g., Xu and McMechan, 1997). Conclusions based on the responses shown above would be strengthened by the presence of diffractions, as the latter tend to be more visible than some of the features that we have discussed. Ideally, migration should be performed to focus and collapse diffractions, to produce more accurately interpretable images (e.g., Fisher et al., 1992).

Some additional numerical experiments were done for which results are not shown here. For example, provided that it is a sufficiently small fraction of a wavelength that it is below the limit of resolution, the thickness of a non-metallic tank/pipe has a negligible effect on the response. In this case, the response is dominated by the contrast between the surrounding soil and the contents of the tank/pipe. Possible ambiguities occur in interpretation when different configurations give similar responses. However, systematic simulation for the most likely configurations will allow both the alternative explanations and the resolution of various features under various conditions to be evaluated.

While this chapter is concentrating on tanks and pipes, the approach of generating a catalog of responses for the situations that are most often expected should prove useful for evaluating the potential of GPR for many other applications in engineering, archeology, sedimentology, geologic and environmental site characterization.

3.8 Appendix to Section 3

Item	Material	Relative dielectric permittivity	Velocity (m/ns)	Conductivity (mS/m)	Q
1	Silty clay	6.0	0.12	6.6	2
2	PCV plastic	3.3	0.16	1.34	7.3
3	Fiberglass	4.8	0.14	0.66	18
4	Air	1.1	0.30	10^{-8}	10^8
5	Pure water	80	0.033	0.01	4800
6	Salt water	80	0.033	5000	0.01
7	Metal	300	0.017	10^{10}	10^{-8}
8	Gasoline	1.94	0.22	10^{-7}	10^8
9	Benzene	2.28	0.2	10^{-7}	10^8
10	Methanol	32.6	0.052	34	0.9
11	DNAPL	2.3	0.19	10^{-7}	10^8

Table 3.1 Material properties used in the simulations. Conductivities are at 100 MHz.

Model no.	Tank material	Contents	Fluid level (%)
1	Fiberglass	Air	100
2	PVC	Air	100
3	Metal	Air	100
4	Fiberglass	Benzene	100
5	Fiberglass	DNAPL	100
6	Fiberglass	Methanol	100
7	Fiberglass	Air/Gasoline	50
8	Fiberglass	Air/DNAPL	50
9	Fiberglass	Air/Methanol	50
10	Fiberglass	Gasoline/Pure Water	50
11	Fiberglass	Air/Pure Water	50
12	Fiberglass	Air/Salt Water	50
13	Fiberglass	Air/Gasoline	70
14	Fiberglass	Air/Gasoline	80
15	Fiberglass	Air/Gasoline	90/95
16	Fiberglass	Water	100

Table 3.2 Material properties used in the simulations. Conductivities are at 100 MHz.
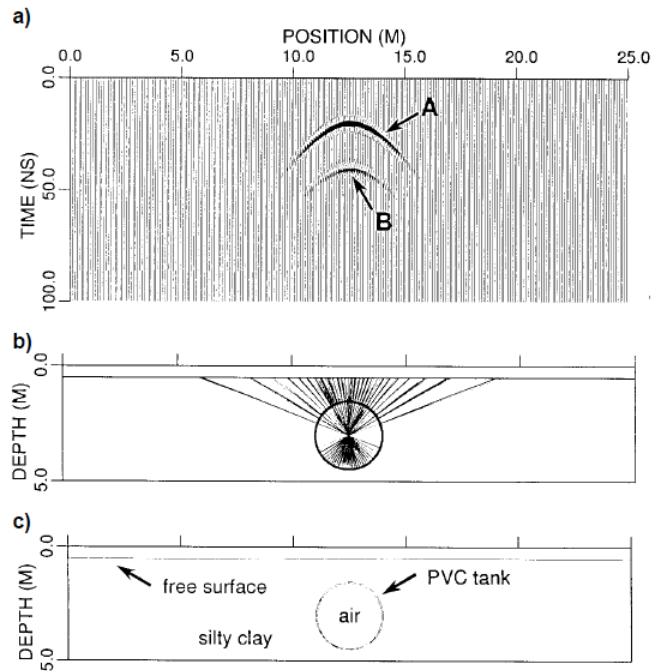
Fig. 3.1 Simulation of the zero-offset GPR response at 200 MHz for a tank model.

Remarks to Figure 3.1: The model parameters are listed in Table 3.1. The synthetic profile (a) is produced by ray tracing (b) through the model (c) to get traveltimes. Amplitudes are computed as described in the text. A and B are reflections from the top and bottom of the tank, respectively. For comparison with the other figures, the amplitude scale factor used for this figure is 160.
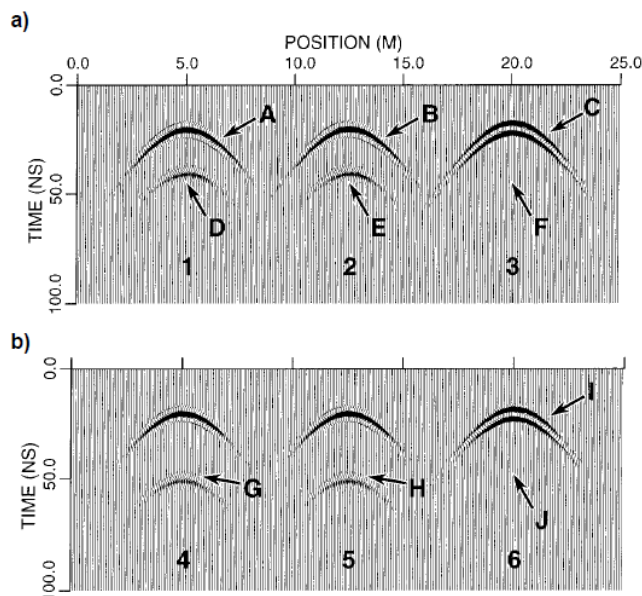
Fig. 3.2 Zero-offset GPR responses as a function of tank material (a) and contents (b).

Remarks to Figure 3.2: Numbers 1–6 refer to the corresponding numbers on the tank configurations in Table 3.2. For comparison with the other figures, the amplitude scale factor used for this figure is 160.
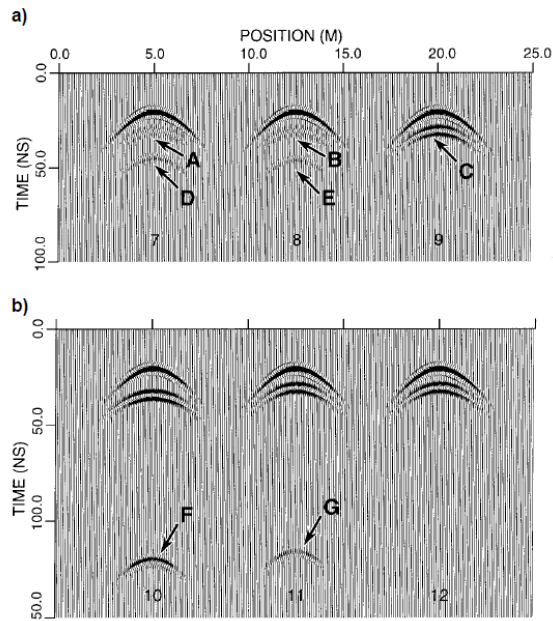
Fig. 3.3 Zero-offset GPR responses of tanks containing two fluids.

Remarks to Figure 3.3: Numbers 7–12 refer to the corresponding numbers on the tank configurations in Table 3.2. For comparison with the other figures, the amplitude scale factor used for this figure is 100.
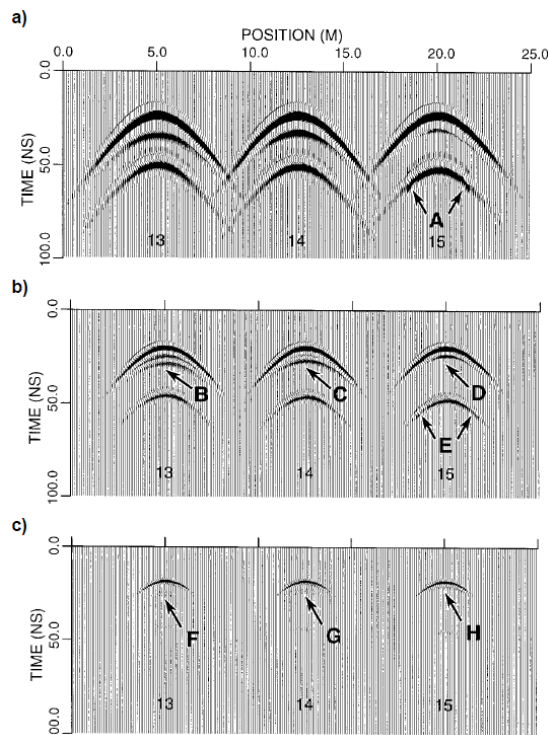
Fig. 3.4 Zero-offset GPR responses of tanks as a function of fluid level and frequency.

Remarks to Figure 3.4: Numbers 13–15 refer to the corresponding numbers on the tank configurations in Table 3.3: (a) are 100 MHz; (b), 200 MHz; and (c), 450 MHz. Models 13, 14, and 15 are 70%, 80%, and 90% full, respectively, except for model 15 in panel (c), which is 95% full (by volume). For comparison with the other figures, the amplitude scale factor used for this figure is 240.

Page20
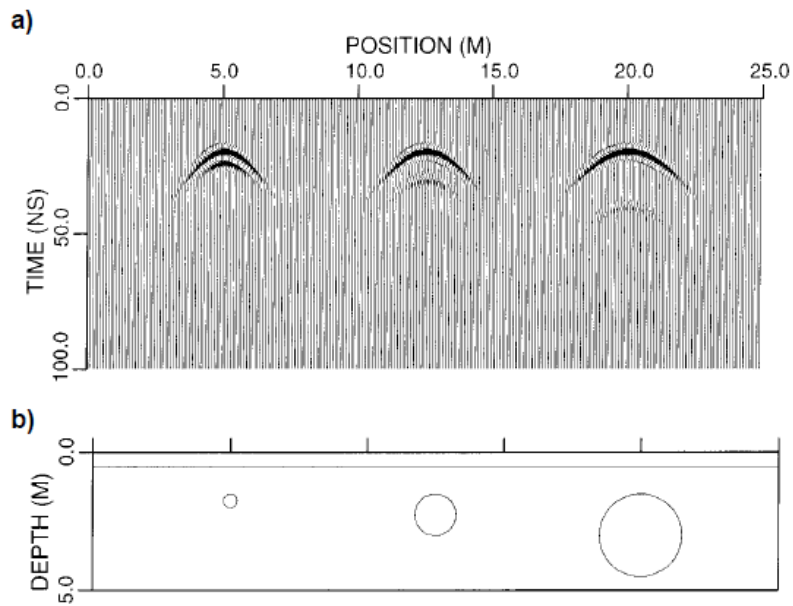
Fig. 3.5 Effects of tank diameter.

Remarks to Figure 3.5: The tank diameters in (b) are 0.5 m (left), 1.5 m (center) and 3.0 m (right). The synthetic responses (a) are for 200 MHz antennas. For comparison with the other figures, the amplitude scale factor used for this figure is 60.
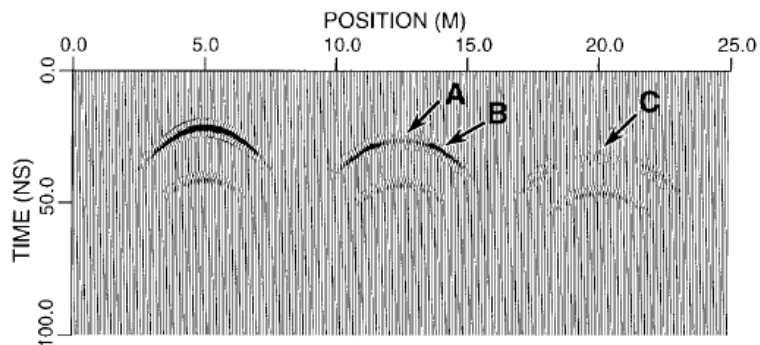
Fig. 3.6 Effects of antenna separation.

Remarks to Figure 3.6: From left to right, the responses are for offsets of 1.0 m, 2.0 m, and 3.0 m. Compare with the zero-offset response of the same model in Figure 3.5. For comparison with the other figures, the amplitude scale factors used in the left, center and right responses are 100, 120, and 250, respectively.
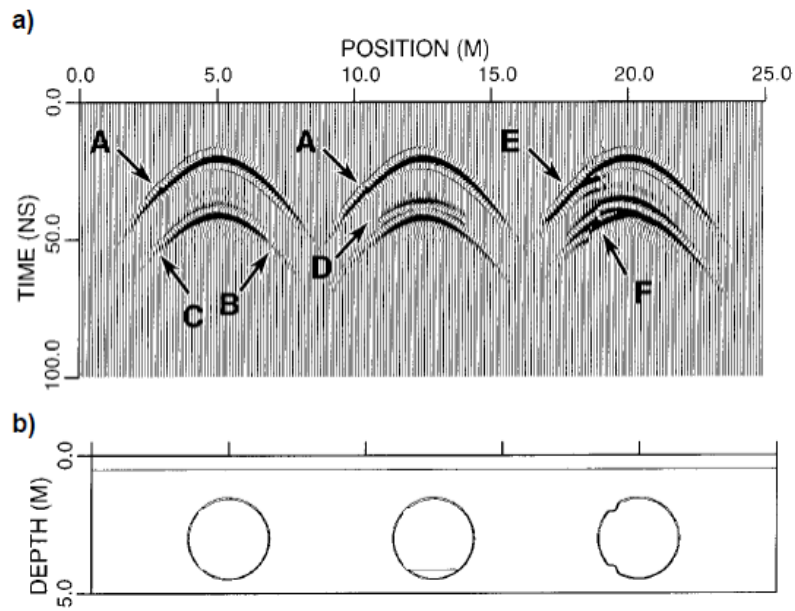
Fig. 3.7 Effects of tank damage.

Remarks to Figure 3.7: From left to right, the models in (b) have two holes, two holes plus residual fluid, and two dents. Compare the synthetic responses (a) with that of the corresponding undamaged tank in Figure 3.1. For comparison with the other figures, the amplitude scale factor used for this figure is 700.

4. GPR SURVEY DESIGN

Ground Penetrating Radar (GPR) is a high frequency electromagnetic sounding technique that has been developed to investigate the shallow subsurface using the contrast of dielectric properties. The method operates on the simple principle that electromagnetic waves, emitted from a transmitter antenna, are reflected from buried objects and detected at another antenna, acting as receiver. GPR data is presented in the form of time-distance plots that are analogous to conventional reflection seismic records, and in fact the method has many similarities to seismic reflection method with a pulse of electromagnetic energy substituting for the elastic (seismic) energy. Nevertheless, the principles and theory of the method are based on the wave equation derived from Maxwell's equations for electromagnetic wave propagation.

The procedure for recording radar sections in the field is similar to other geophysical profiling and sounding techniques. Effective ground penetrating radar surveys involve considerable planning if the surveys are to meet pre-defined objectives. The most important step in a ground penetrating radar survey is to clearly define the problem. This step is not unique to radar but common to all geophysical techniques although often overlooked in the urge to <rush off and collect data>. There are six main parameters to define for common-offset, single-fold GPR reflection surveys:

Operating frequency – Election of the handling frequency for a radar survey is not simple. There is a compromise between spatial portability. As a rule, it is better to trade off resolution for penetration. Obviously, there is no use in having great resolution if the target cannot be reached. A simple guide is to use the following formula:

$$\log_e f = -0.95 \log_e z + .15$$

Where f is the operating frequency and z is the required depth of investigation.

Estimating the time window – the way to estimate the time window (tw) required is to use the expression

$$tw = 1.3 \frac{2z}{v}$$

where the maximum depth and minimum velocity likely to be encountered are used. The above expression increases the estimated time by 30% to allow for uncertainties in velocity and depth variations. If no information is available on the electrical properties of the study area, a first estimate will be obtained from tables in function of the porosity and moisture content of the predominant lithology.

Sampling interval – one of the parameters utilized in designing radar data acquisition is the time interval between points on a recorded waveform. The sampling concept should be at most half the period of highest frequency signal in the record. Nevertheless, for good survey design, the sampling rate should be approximately six times the centre frequency of the antenna being utilized. The function relationship is

$$t = \frac{1000}{6f}$$

where f is the centre frequency in MHz and t is time in ns.

In some instances it may be possible to increase the sampling interval slightly beyond what is quoted, but this should one be done when data volume and speed of acquisition are at a premium over integrity of the data.

Antenna separation – Most GPR systems adopt separate antennas for transmitting and receiving (commonly referred to as bistatic operation). The ability to vary the antenna spacing can be a powerful aid in optimizing the system for specific types of target detection. To maximum target coupling, antennas should be spared such that the refraction focusing peak in the transmitter and receiver patterns point to the common depth to be investigated. Increasing the antenna separation also increases the reflectivity of flat lying planar targets that can sometimes be advantageous.

Antenna orientation – In general, the antennas used for GPR are dipolar and radiate with a preferred polarity. The antennas are normally oriented so that the electric field is polarized parallel to the long axis or strike direction of the target.

Station spacing – The selection of spacing between discrete radar measurements is closely linked to the centre operating frequency of the antennas and to the dielectric properties of the subsurface materials involved in order to assure the ground response is not spatially aliased, the Nyquist sampling intervals should not be exceeded.

5. POST-ACQUISITION PROCESSING AND INTERPRETATION

The degree of post-acquisition processing of GPR data is dependent on the objectives of the investigation. Most of the post-processing techniques available for the reflection seismic method are also useful for GPR data analysis. Nevertheless, there is a danger in making the comparison of radargrams to seismograms that the vector nature of radar may be overlooked. So incorrect assumptions are made about the way the radiowaves behave in geologic media. While seismic data processing can be used effectively in most cases, the electromagnetic polarisable characteristics of the radiowaves are analogous to seismic S-waves that to P-waves. The main post-processing and interpretation techniques are:

Gain recovery – When radar waves propagate into the subsurface by way of transmission reflection and refraction, its electromagnetic energy is severely attenuated not only by spatial spreading but also by the earth's conductivity. Consequently, the amplitude of the signal is much smaller in the later time. Gain recovery is designed to rescue this time dependent attenuation. These are several mathematical gain procedures.

> AGC (Automatic Gain Control) attempts to equalize all signals by applying a gain, which is inversely proportional to the signal strength. This type of gain is most useful for defining continuity of reflecting events.

> SEC (Spreading and Exponential Compensation) is a composite of a linear and an exponential time again.

Filtering - The main objective of filtering in GPR processing is to remove undesired noise from the records, leaving ideally only meaningful reflections.

> Trace-to-trace averaging: this processing option, as what the name implies, adds two or more traces to produce an average trace (moving average). The primary purpose of this type of processing is to emphasize flat lying or slowly dipping reflectors while suppressing rapidly changing ones acting as a spatial low pass filtering.

> Down-to-trace averaging: this option performs signal averaging by replacing the data at a given point by the average over a window centered about that point. This type of averaging acts as a low pass temporal filter by reducing random noise though averaging.

> Trace-to-trace differencing: in this processing each trace is replaced by the difference between itself and the previous trace (except for the first trace). This filter has the effect of enhancing rapidly changing features in the profile and suppressing flat lying or constant features. This filter is a simple high spatial filter.

> Delete mean trace: this filter is used to eliminate ringing and horizontal multiples from the radar image. When applied, this filter calculates a mean trace in time domain over a selected area, which is then subtracted from all the traces in the image. Normally a large number of traces must be included.

> Frequency domain filtering: three kinds of filtering can be performed in the frequency domain: low-cut, high-cut and band-pass filtering.

Modeling - GPR analysis is greatly assisted by forward modeling in which theoretical (synthetic) radargrams are constructed for layered models in order to derive insight into physical significance

of reflection events contained in radar sections. An important use of synthetic radargrams is in studying the effect of changes in the layering on the record. Three main modeling techniques are available: 1D modeling, ray path modeling, F-K modeling. Where the structure and/or horizontal velocity variation are complicated, iterative ray tracing may be used to determine a model that is compatible with the radar observations. The usual assumption is that reflections mark the boundaries between layers, each of which has constant velocity.

Zero offset modeling: this procedure uses a two-dimensional ray tracing approach assuming the transmitter and receiver are coincident. Both attenuation and velocity and can be varied in any zone. The model allows variable surface topography and incorporates the antenna pattern. This model does not address diffraction and evanescent wave features as well as multiple reflection.

Finite offset modeling: as in the previous case, this procedure also uses a two-dimensional ray tracing approach but permits any transmitter/receiver separation.

F-k modeling - this procedure uses a two-dimensional Fourier approach transform single or continuous lines of point reflectors in uniform velocity, zero attenuation background into the equivalent time-position radar section. This model fully incorporates different events.

Migration - The purpose of migration is to transform GPR waveforms into an accurate picture of subsurface geology. As in the reflection seismic method, GPR profiles are migrated because subsurface reflecting points do not necessarily lie vertically beneath surface observation points. An operational definition of computer migration is: a space and time variant filtering process which maps observed space-time amplitude data into either time or depth with correct amplitudes at true spatial positions.

The main reasons for migrate GPR profiles are:

- Correct structural placement of dipping events;

- Focus diffractions caused by point scattering centres and subsurface fault bounds;

- Correct amplitudes for geometric focusing effects and spatial smearing;

- Sorting out of crossing events like those produced by sharp synclines;

- Improvement in resolution.

Straitigraphic interpretation - Identification of significant anomalies on GPR records is a pattern recognition process that consists of recognizing reflection features that are characteristic of specific geological environment are essential for interpreting the radar images. In analogy to seismic facies, radar facies is defined as the sum of all characteristics of a reflection pattern produced by a specific formation. Thus radar facies refers to differences in appearance of radargram and radar reflections respond to both structural and textural features. These effects, called radar facies elements are:

Reflection amplitude;

Dominant frequency;

Reflection configuration;

Reflection continuity;

External form (geometry) of radar facies unit;

Reflection polarity;

Abundance of reflections;

Degree of penetration.

Time slices – 3D GPR data can be considered as volume and therefore can be sliced in various ways. The data sliced horizontally provides time slices that allow the interpreter to generate amplitude contour maps with considerable ease and accuracy. Some interactive software packages enable to interpret effectively and efficiently 3D radar data.

6. APPLICATION OF GPR

Ground penetrating radar has been demonstrated to be a valuable tool in groundwater studies, hazardous waste investigations, mapping sediment sequences and many other applications. The chapter summarized three typical categories which are applied for infrastructure.

Engineering applications – In geotechnical applications, GPR can be used to detect disturbed soils and backfills as well as to locate void and delimitations beneath concrete structures, e.g. bridge decks, highways, and airport pavements (Benson, 1995). These objects exhibit markedly different electrical properties compared to surrounding materials.

Conduit and pipe detection – GPR is frequently used to locate features such as buried tanks and pipes (Zeng and McMechan, 1997), reinforcing not in concrete structures, and conduits embedded in the ground for water, sewer, electrical cable or gas connections (Hayakawa and Kawanaka, 1998). Locating underground pipes for efficient pipe system management and for avoiding damage during excavation has become a relevant issue in metropolitan areas. The increasing use of trenchless techniques for underground pipe laying has opened a new field for the applications of ground penetrating radar. Before the drilling begins, the geological conditions and the positions of existing utilities have to be known because otherwise they could be damaged or destroyed. Most horizontal drilling projects in urban areas take place within a depth of 3 m, but as the available maps are not accuracy, GPR can assist the horizontal drilling technique by predicting obstacles and avoiding damages.

Road Inspection practice – in recent years, GPR inspection of roads has evolved as a powerful technique offering several advantages when compared to traditional methods. In particular it is non-destructive, the results are quasi-continuous and data can be acquired at high rates (Davis et al., 1994). Traffic obstructions can be minimized or avoided. Important applications are the inspection of pavement layer thickness and pavement damages, the investigation of sub-pavement structures and locating reinforcement bars and damage in concrete structures such as bridges. The comparison between two data sets obtained before and after rehabilitation work suggests the suitability of GPR as a tool for quality control.

Reference

1) Albert C., Victor, P., Lluis R., 2000, Fundamentals of ground penetrating radar in environmental and engineering applications: Annali Di Geofisica, v. 43, n. 6, p. 1091-1103.

2) Annan, A.P., Scaife, J. E., and Giamou,P., 1990, Mapping buried barrels with magnetics and ground-penetrating radar: 60th Ann. Internat. Mtg., Soc. Expl. Geophys., Expanded Abstracts, p. 422–423.

3) Annan, A. P., 1973, Radio interferometry depth sounding: Part 1— Theoretical discussion: Geophysics, v. 38, p. 557–580.

   A. Novo, M. Grasmueck,D. Viggiano, H. Lorenzo, 2008, 3D GPR in Archeology: What can be gained from dense Data Acquisition and Processing?, Proc. 12th International Conference on Ground Penetrating Radar (GPR 2008), Birmingham, UK, p. 5.

4) Barringer, A. R., 1965, Research directed to the determination of subsurface terrain properties and ice thickness by pulsed VHF propagation methods: Air Force Cambridge Research Laboratories contribution AF19(628)2998.

5) Barringer, A. R., 1966, The use of audio and radio frequency pulses for terrain sensing: in Selected papers on remote sensing of the environment, reprinted by American Society of Photogrammetry, p. 215-226.

6) Beres, M. and F. P. Haeni, 1991, application of ground penetrating radar method in hydrogeologic studies, Ground Water, v. 29(3), p. 375-386.

7) Brewster, M. L. and A. P. Annan, 1994, ground penetrating monitoring of a controlled DNAPL release: 200 MHz radar, Geophysics, v. 59(8), p. 1211-1221.

8) Cai, J., and McMechan, G. A., 1995, Ray-based synthesis of bistatic ground penetrating radar profiles: Geophysics, v. 60, p. 87–89.

9) Caldecott, R., 1967, Electromagnetic Pulse Sounding for Surveying Underground Water: Electroscience Laboratory, Ohio State University, Columbus, OH, Report 401X-1, 429p.

10) Caldecott, R., Irons Jr, D. A., Moffatt, D. L., Peters Jr, L., Puskar, R. J., Toth, J. F. and Young,

11) Clarke, G. K. C., 1987, A short history of scientific investigations on glaciers: J. Glaciol., spec. issue commemorating the fiftieth anniversary of the International Glaciological Society, p.4-24.

12) Czarnowski, J., Heinze, S., Bruhl, P., Staib, C., Robeck, M., Frank, G., and Fruhwirth, Dr. R., 1994, Pipeline projects in Germany using GPR: Proc. 5th Internat. Conf. on GPR, Expanded Abstracts, Univ. of Waterloo, p. 1107–1113.

13) Davis, J.L., J.R. Rossiter., D.E. Mesher and C.B. Dawley, 1994, Quantitative measurement of pavement structures using radar, in proceedings of the 5th international conference on Ground Penetrating Radar, Kitchener, pp. 319-334.

14) Engheta, N., Papas, C. H., and Elachi, C., 1982, Radiation patterns of interfacial dipole antennas: Radio Sci., v. 17, p. 1557–1566.

15) Graf, F. L., 1989, Use of ground-penetrating radar to pinpoint natural gas pipeline leaks: 59th Ann. Internat. Mtg., Soc. Expl. Geophys., Expanded Abstracts, p. 226–228.

16) J. D., 1972, Electromagnetic pulse sounding for surveying underground water: Ohio State University Electroscience Laboratory Report 401X-1, 81p.

17) M. Grasmueck, R. Weger, and H. Horstmeyer, 2005, Full-Resolution 3D GPR Imaging, Geophysics, v. 70, p. K12-K19.

18) M. Grasmueck and D. Viggiano, 2006, 3D/4D GPR Toolbox and Data Acquisition Strategy for High-Resolution Imaging of Field Sites," in Proc. 11th International Conference on Ground Penetrating Radar (GPR 2006), Columbus, OH , p. 6.

19) Morey, R. M., 1974, Continuous subsurface profiling by impulse radar: in Proceedings of the Engineering Foundation Conference on Subsurface Exploration for Underground Excavation and Heavy Construction, Henniker, NH, August 11-16, 1974, American Society of Civil Engineers, p. 213-232.

20) Powers, H. M., and Olhoeft, G. R., 1996, Modeling the GPR response of leaking, buried pipes: Proc. SAGEEP, Env. Eng. Geophys. Soc., Expanded Abstracts, p. 525–534.

21) Simmons, G., Strangway, D. W., Bannister, L., Baker, R., Cubley, D., La Torraca, G. and Watts, R., 1972, The surface electrical properties experiment: in Lunar Geophysics, Z. Kopal and D. W. Strangway, eds., Dordrecht, D. Reidel, p. 258-271.

22) Smith, D. G. and H. M. Jol, 1997, Radar structure of a Gilbert-type delta, Peyto Lake, Banff National Park, Canada, Sediment, Geol., v. 113(3-4), p. 195-209.

23) Stern, W., 1929, Versuch einer elektrodynamischen Dickenmessung von Gletschereis: Ger. Beitr. zur Geophysik, v. 23, p. 292-333.

24) Stern, W., 1930, Uber Grundlagen, Methodik und bisherige Ergebnisse elektrodynamischer Dickenmessung von Gletschereis: Z. Gletscherkunde, v. 15, p. 24-42.

25) Stockbauer, F. S., and Kalinec, J. A., 1995, Real-time interpretation of EM-31 and GPR data for expedited site investigation: Proc. SAGEEP, Env. Eng. Geophys. Soc., Expanded Abstracts, p. 671–676.

26) Tong, L. T., 1993, Application of ground-penetrating radar to locate underground pipes: Terr. Atm. Ocean Sci., v. 4, p. 171–178.

27) W.L. Lai, S.C. Kou, W.F. Tsang and C.S Poon, 2009, Characterization of concrete properties from dielectric properties using ground penetrating radar, Cement and Concrete Research 39 (2009), pp. 689-695.

28) Young, J. D., 1996, Radar history: invited plenary lecture, GPR '96, 6th International Conference on Ground Penetrating Radar, Sept 30-Oct 3, Sendai, Japan, this volume.

29) Zeng, X., McMechan, G. A., Cai, J., and Chen, H. W., 1995, Comparison of ray and Fourier methods for modeling monostatic ground penetrating radar profiles: Geophysics, v. 60, p. 1727–1734.

30) Zeng, X. and G.A McMechan, 1997, GPR characterization of buried tanks and pipes, Geophysics, v.62(3), pp. 797-806.

31) Zeng, X., G.A. McMechan, J. Cai and H.W. Chen, 1995, Comparison of ray and Fourier methods for modeling monostatic ground penentrating radar, Geophysics, v60, pp. 1717-1734.

Appendix A: Abbreviations

Company/ Organization	
Code	**Description**
BD	Buildings Department, HKSARG
CEDD	Civil Engineering and Development, HKSARG
DSD	Drainage Services Department, HKSARG
EMSD	Electrical and Mechanical Services Department, HKSARG
EPD	Environmental Protection Department, HKSARG
HA	Hong Kong Housing Authority, HKSARG
HKIUS	Hong Kong Institute of Utility Specialists
HKURC	Hong Kong Utility Research Centre
HyD	Highways Department, HKSARG
LandsD	Lands Department, HKSARG
LD	Labour Department, HKSARG
PolyU	The Hong Kong Polytechnic University
UTI	Utility Training Institute
WRc	Water Research Centre
WSAA	Water Services Association Australia
WSD	Water Supplies Department, HKSARG
WTI	Water Training Institute
Others	
Code	**Description**
%	Percentage
BMP	Bitmap (Picture Format)
BWCS	Buried Water Carrying Service
CCE	Conduit Condition Evaluation
CCE(CCTV & ME)	Conduit Condition Evaluation(Closed Circuit Television & Man- Entry)

Company/ Organization	
CCES	Conduit Condition Evaluation Specialists
CCTV	Closed Circuit Television
CD	Compact Disc
CL	Cover Level
COP	Code of practice
CP	Competent Person
DN	Nominal Diameter
DP	Design Pressure
DVD	Digital Versatile Disc
e.g.	Exempli Gratia
GIS	Geo-Information System
EPR	Environmental Protection Requirements
etc.	et cetera
GL	Ground Level
H	Height
HKCCEC	Hong Kong Conduit Condition Evaluation Codes
HPWJ	High Pressure Water Jetting
hr	Hour
Hz	Hertz
ICG	Internal Condition Grade
ID	Internal Diameter
IDMS	Integrated Data Management System
IL	Invert Level
ISO	International Standards Organization
JPEG	Joint Photographic Experts Group (Picture Format)
kHz	Kilo- Hertz
kPa	Kilopascal

Company/ Organization	
m	Meter(s)
ME	Man Entry
MHICS	Manhole Internal Condition Survey
mm	Millimetre(s)
Mpa	Megapascal
MPEG	Motion Picture Experts Group (Video Format)
MS	Method Statement
MSCC	Manual of Sewer Condition Classification, UK
OHSAS	Occupational Health and Safety Assessment Series
PPE	Personal Protective Equipment
ppm	Parts per million
PS	Particular Specification
PSI	Pound Per Square Inch
QA/ QC	Quality Assurance/ Quality Control
Ref.	Reference
RMSE	Root Mean Square Error
RPUS	Recognized Professional Utility Specialist
RTO	Recognized Training Organization
SCG	Service Condition Grades
SOPs	Safe Operator Procedures
SPF	Sun Protection Factor
SPG	Structural Performance Grade
SRM	Sewer Rehabilitation Manual
STP	System Test Pressure
TTA	Temporary Traffic Arrangement
US	Utility Specialist
VHS	Video High Speed

Company/ Organization	
W	Width
WLD	Water Leakage Detection
WO	Works Order
WP	Work Procedure

Utility Training Institute (UTI)
Suite 209, Favor Industrial Centre,
2-6 Kin Hong Street,
Kwai Chung, New Territories
HKSAR, China

Tel: (+852) 2690 3899   Fax: (+852) 2618 4500   Email: info@uti.hk

Guideline Amendment Form

Please fill in the following form if any error or mistake is found in this manual. We thank for your support and appreciate your continuous help in improving this manual.

Discipline*	Page No.	Description of Existing Content	Suggested Amendment

*
A. Conduit Condition Evaluation (CCTV and ME Survey)
B. Manhole Internal Condition Survey
C. Utility Survey (Pipe Cable Locator Survey, PCL)
D. Water Leakage Detection and Control
E. Advanced Leakage Detection of Buried Water Carrying Services Affecting Slopes
F. Pipe Rehabilitation by Trenchless Technology
G. GPR(Ground Penetrating Radar) Survey
H. Flow Study in Drainage Conduit (流量監控)
I. Pipe Condition Surveys by other non-destructive methods
J. Data Management for Utility Records
K. Utility Management
L. Safety

Please fill in your contact information in case follow up is needed.

First Name: _____ Second Name: _____ Last Name: _____

Title: _____

Organization: _____

#Telephone No.: _____ #Email Adress: _____

#Address: _____

Please fill in one or more contact information in the blanks provided
This amendment form is available at: www.uti.hk

G P R